JOURNAL OF SPACECRAFT AND ROCKETS
Vol. 42, No. 4, July–August 2005

Design and Testing of a Control Moment Gyroscope Cluster for Small Satellites

V. Lappas,* W. H. Steyn,† and C. Underwood‡
University of Surrey, Guildford, England GU2 7XH, United Kingdom

Experimental results on the performance of a control moment gyroscope cluster are presented. The goal is to design and evaluate a control moment gyroscope cluster for three-axis control for agile small satellites. The experimental data are compared with simulation (theoretical) results and both are used to verify the principles, advantages, and performance specifications of a control moment gyroscope cluster for a small satellite, in a practical way. Control moment gyroscope systems are considered in the literature to be more efficient devices, from an electrical power point of view, than current actuators such as reaction/momentum wheels. Experimental measurements are presented and then compared to two reaction wheels of different size. Control moment gyroscopes are shown to have a potential performance advantage over reaction/momentum wheels for spacecraft with agile requirements.

Nomenclature

$\boldsymbol{H}$	=	observation matrix
$\boldsymbol{h}$	=	control moment gyroscope (CMG) angular momentum vector, N · m · s
h_0	=	CMG angular momentum, N · m · s
I_{AB}	=	air-bearing moment of inertia, kg · m^2
I_{CMG}	=	flywheel moment of inertia, kg · m^2
I_{RW}	=	reaction wheel moment of inertia, kg · m^2
I_s	=	spacecraft moment of inertia, kg · m^2
$\boldsymbol{K}$	=	Kalman gain
$\boldsymbol{N}_{\text{CMG}}$	=	CMG torque vector, N · m
N_d	=	external disturbances, N · m
N_{RW}	=	reaction wheel torque, N · m
N_z	=	Z-axis CMG experimental torque, N · m
$\boldsymbol{P}_k$	=	covariance matrix
$\hat{\boldsymbol{P}}_k$	=	covariance matrix update
P_{act}	=	actuator electrical power, W
$\boldsymbol{q}_\omega$	=	estimate of angular noise, rad/s
$\dot{\boldsymbol{q}}_\omega$	=	estimate of angular acceleration noise, rad/s^2
R	=	estimate of angular rate measurement noise, (rad/s)^2
t_m	=	time to complete maneuver, s
β	=	CMG pyramid skew angle, deg
$\boldsymbol{\delta}$	=	gimbal angle vector, deg
ε	=	scaled energy index, J/kg · m^2
θ	=	air-bearing rotation angle, deg
$\boldsymbol{\omega}$	=	angular rate vector, rad/s
ω_{AB}	=	air-bearing angular speed, rad/s
$\bar{\boldsymbol{\omega}}_k$	=	intermediate angular rate state vector, rad/s
$\dot{\bar{\boldsymbol{\omega}}}_k$	=	intermediate angular acceleration state vector, rad/s^2
ω_w	=	flywheel speed, rad/s
ω_z	=	angular rate of air bearing, rad/s
ω_0	=	angular rate initial value, rad/s

Received 27 December 2003; revision received 29 June 2004; accepted for publication 17 July 2004.

*Lecturer in Attitude/Orbit Control Systems, Surrey Space Centre, School of Electronics and Physical Sciences.

†Team Leader, ADCS Team, Surrey Satellite Technology, Ltd.; currently Professor, Department of Electrical Engineering, University of Stellenbosch, Stellenbosch, 7602, South Africa.

‡Reader, Surrey Space Centre.

Introduction

A SINGLE-GIMBAL control moment gyroscope (SGCMG) is a control moment gyroscope (CMG) with a constant-speed momentum wheel, gimbaled in one axis only. For full three-axis control of a spacecraft, a cluster of four CMGs is normally used. CMGs, due to their inherent gyroscopic properties, can potentially generate large torque and angular momentum outputs in a more efficient way than current technologies such as reaction or momentum wheels. Depending on the gimbal axes, a CMG can be distinguished as either an SGCMG or a double-gimbal CMG. The type and number of CMGs that can be used in an attitude control system (ACS) is a tradeoff among performance, cost, and mechanical and algorithm complexity. SGCMGs and variable-speed CMGs are the most powerful of all (from the torque point of view) but SGCMGs require a minimum of four units for full three-axis control to avoid singularities.[1,2] SGCMGs (referred to as CMGs in this work) are the main consideration in this paper.

CMGs have been thoroughly studied in the past and have been baselined to be used in future space missions.[3–8] CMGs can potentially change the way in which we will develop and operate the small satellites of the future. Agility, besides increasing the operational envelope of the spacecraft, will also enable such spacecraft to collect more Earth and space science data than before while using the same or even fewer resources. This in practice means a direct increase in the commercial and scientific value of these spacecraft. Small satellites are bound to face some challenging missions in the future that will require a high degree of agility (high slew rates). The motivation of this work is to explore the possibility of employing CMGs on small satellites, enabling new missions and also increasing their operational envelope and enhancing their commercial and scientific value. However, to date, CMGs have never been used on small satellites, due to the complexity, high cost, and limited onboard resources on small spacecraft. Developments in miniature commercial off-the-shelf (COTS) microelectronics and an innovative design can potentially make CMGs possible for a small satellite. The paper examines the technical feasibility of developing such an actuator and attempts to validate and evaluate these actuators and their performance on a microsatellite.

New space missions have as one of their major design requirements the feature of agility.[1–8] Most of the current CMG developments[4–8] are focused on medium-size spacecraft, in the 1-ton class for Earth-observation platforms. The two CMGs available for these platforms are the Honeywell M50 CMG and the Astrium CMG 15-45S. The Honeywell CMG capitalizes on the wide range and experience of Honeywell for large CMGs that have flown on a number of military-related missions.[1,2] Astrium's CMG 15-45S has been developed for the Pleiades constellation, a series of

optical and radar agile spacecraft to be flown in 2006.[5] With total masses exceeding 15 kg, these actuators, although powerful, would be too heavy to be used on small satellites (<500 kg) and expensive. A smaller CMG, designed by the University of Surrey, has been designed and is in orbit as part of the BILSAT-1 enhanced microsatellite experimental payload suite.[3] The two-CMG cluster is used to test agile pitch-axis control for stereoscopic imaging.[3]

The work presented in this paper focuses on exploring the feasibility, design, and evaluation of CMGs for an agile three-axis microsatellite. Specifically the main aims are to practically confirm the theoretical work (simulations) performed in previous studies and to validate the viability of using CMGs as actuators on a microsatellite in a practical way. Furthermore, the experimental work is used to confirm the agility and power efficiency that CMGs can potentially provide to microsatellites. The work following is structured as follows. First the CMGs are sized for a University of Surrey microsatellite platform,[1] and then the design of the CMGs is presented. Details of the CMG experiments are presented along with a discussion of the results and the sources of experimental error. Finally an analysis on the electrical power consumption of the CMGs is presented along with a comparison to reaction wheel (RW) actuators currently in orbit.

CMG Sizing and Design

The four-CMG cluster in pyramid configuration discussed throughout many CMG studies is used as the basis for an ACS system for a microsatellite.[1,2] From analyses conducted, it was concluded that a torque of 52.25 mN · m is required to perform a 30-deg maneuver in 10 s.[1] This requirement is used to size a CMG for a microsatellite:

$$\boldsymbol{N}_{\mathrm{CMG}} = \boldsymbol{h} \times \dot{\boldsymbol{\delta}} \tag{1}$$

where $\boldsymbol{h}$ is the CMG angular momentum vector and $\dot{\boldsymbol{\delta}}$ is the gimbal rate vector of the CMG cluster. Sizing the angular momentum of the CMG, $\boldsymbol{h}$, and the maximum gimbal angles rate, $\dot{\delta}_{\max}$ (same for all four CMGs), is a tradeoff among performance (torque), size, angular rate profile, hardware constraints, and singularity avoidance. One would want to keep the angular momentum as small as possible because it depends on the inertia of the spinning wheel as well as the speed of rotation of the wheel. This implies that, with a larger angular momentum, a larger flywheel motor will be required, with a heavier disk. On the other hand, the larger the gimbal rate, the larger the gimbal angle excursions, thus, the greater the probability that the CMGs will enter into a singularity. Thus, it becomes important to optimize $\boldsymbol{h}$ and $\dot{\delta}$ given the mechanical constraints of a practical system. An attitude control model designed in previous studies[1] is used to perform and evaluate this trade and to select the optimum values to be used in a CMG system. From simulations and evaluation of available COTS hardware, it has been decided to use a gimbal rate of 7.5 deg/s (or 0.13 rad/s). Normally, one can calculate the angular momentum $\boldsymbol{h}$ by using Eq. (1) (and get h_0 of each CMG) but this will not enable us to properly size a CMG for a single-axis maneuver. This requires analyzing a single-axis maneuver (x axis) for the CMG cluster. For this maneuver, the torque generated will be (Fig. 1)

$$\boldsymbol{h}_1 = h_0 \begin{bmatrix} -\sin\delta_1 \cos\beta \\ \cos\delta_1 \\ \sin\delta_1 \sin\beta \end{bmatrix}, \qquad \dot{\boldsymbol{\delta}}_1 = \begin{bmatrix} \dot{\delta}_1 \sin\beta \\ 0 \\ \dot{\delta}_1 \cos\beta \end{bmatrix}$$

By taking the cross product, $N_{1x} = h_0 \dot{\delta}_1 \cos\beta \cos\delta_1$,

$$\boldsymbol{h}_2 = h_0 \begin{bmatrix} \sin\delta_2 \cos\beta \\ -\cos\delta_2 \\ \sin\delta_2 \sin\beta \end{bmatrix}, \qquad \dot{\boldsymbol{\delta}}_2 = \begin{bmatrix} \dot{\delta}_2 \sin\beta \\ 0 \\ -\dot{\delta}_2 \cos\beta \end{bmatrix}$$

Again, the cross product is $N_{2x} = h_0 \dot{\delta}_2 \cos\beta \cos\delta_2$. Because of symmetric rotation, $\delta_1 = \dot{\delta}_2$ and $\dot{\delta}_1 = \dot{\delta}_2 = \dot{\delta}$:

$$N_x = 2h_0 \dot{\delta} \cos\beta \cos\boldsymbol{\delta} \tag{2}$$

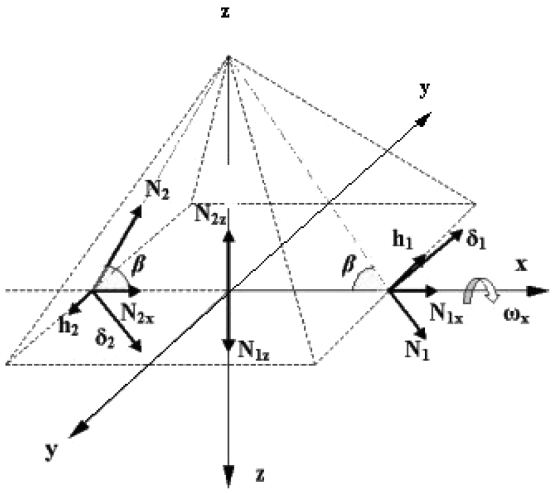

Fig. 1 CMG cluster for an *x*-axis maneuver.

Thus, for $N_z = 52.25$ mN · m, $\dot{\delta} = 0.13$ rad/s and $\boldsymbol{\delta} = 0$ deg, $h_0 = 0.347$ N · m · s. A value of 0.35 N · m · s is used to size the disk of the spinning wheel:

$$h_0 = I_{\mathrm{CMG}} \omega_w \tag{3}$$

The dc motor chosen to be used to spin the disk has a maximum speed of rotation of 20,000 rpm. Thus, a disk with an inertia of 1.7×10^{-4} kg · m^2 is needed. A more detailed analysis on the CMG sizing and performance analysis can be found in Ref. 1.

CMG Design

The design and testing of a preprototype CMG [CMG Mark (Mk) I] in previous work[1] led to the design of an enhanced CMG as part of a four-CMG cluster, the CMG Mk II, which is used in the experiments in this work (Fig. 2). Both CMGs use space-compatible COTS components. The CMG Mk II utilizes a powerful flywheel motor with integrated electronics (Faulhaber 1525 BRE), a larger flywheel (angular momentum), properly sized to generate the required torque on the Mk II CMG ($I_{\mathrm{CMG}} = 1.7 \times 10^{-4}$ kg · m^2), and electronics based on a C515 microcontroller. The Mk II version focuses on resembling as much as possible a future CMG ACS system for the 50-kg-microsatellite model used throughout this analysis.

In this context, the CMG electronics are designed based on the architecture used on Surrey's small satellite designs. A C515 micro controller is used to "translate" via a control area network (CAN) bus various telecommands which enable the gimbal motors to operate. A personal computer is used to send telecommands to and receive telemetry from the CMG cluster. Different gimbal rates can also be produced, resulting in different gimbal angle excursions and, thus, different torque outputs. An improved and more robust mechanical design is also implemented in the CMG Mk II design. The design consists of simple yet robust mechanical components to support the CMGs. Two supports are used to mount the gimbal and flywheel motors. Bearings provide further support to each CMG unit (two per unit) and couplers (two per unit) are used to connect rotating components. Potentiometers are used to provide measurements of the rotating structure of the CMGs. The CMG Mk II electronics are designed with the same architecture used in most of the UoSAT small satellites. Its processor is based on the Siemens C515 microprocessor. Four Motorola MC3479 stepper motor integrated circuits (ICs) are used to power the four stepper (gimbal) motors. These ICs are connected to the C515 microcontroller as depicted in Fig. 3. To command the CMGs to operate, a simple computer program implements tasks to send and receive CAN telemetry, telecommand, and file transfer protocols.[1]

In this program, simple executables (e.g., telecommands) are designed to make the CMGs operate with the desired gimbal rates

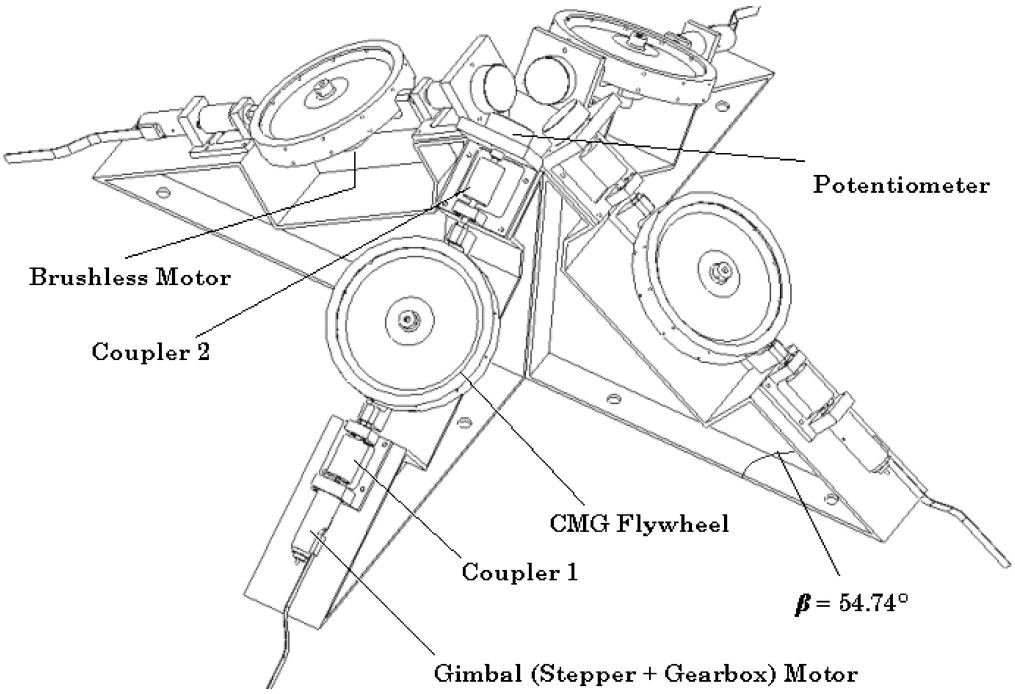

Fig. 2 CMG Mk II cluster diagram.

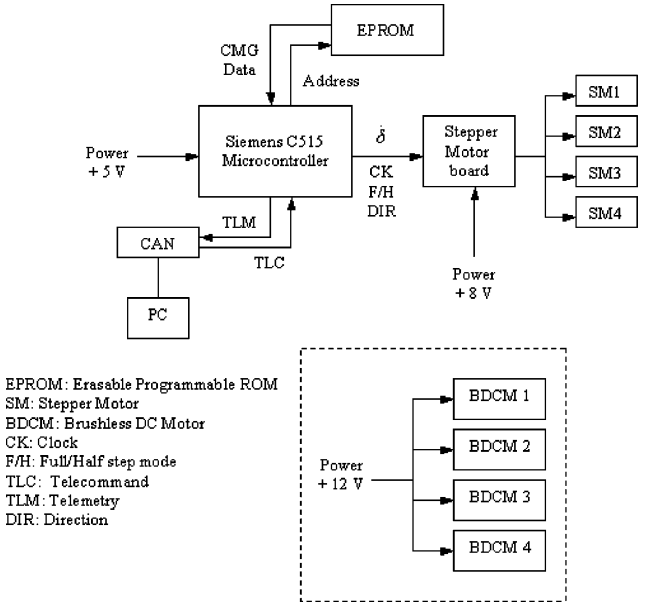

Fig. 3 Detailed CMG electronics block diagram.

(positive/negative) and direction (clockwise/counterclockwise). The telecommand is then processed through the CAN card and is intercepted by the C515 microprocessor. A CMG program on the C515 board is then used to communicate the telecommands to the stepper (gimbal) motors. The CMG program used is composed of a main processor loop, which executes a number of tasks concurrently. The main processor loop reads the telecommands and performs them accordingly. These include displaying the gimbal angle values and setting the gimbal rates and step mode according to the executables that have been written.

CMG Cluster Experiments and Results

Having designed the electronics to control the flywheel motor and gimbal motors, the CMG is put on an air-bearing table. An air-bearing table provides the capability of rotation without significant friction. It is frequently used to test the dynamic characteristics and performance of a model satellite control system during the prelaunch experimental testing campaign on the ground. It is suspended by air, which allows nearly frictionless rotation. The rotational freedom depends on the mechanical structure. The air-bearing table used is a single-degree-of-freedom air bearing mounted around a semisphere that provides air suspension via six holes, placed 120 deg apart in two different levels, which propel air under pressure to slightly lift the rotating part of the table from the stationary part. The resulting lack of contact between the rotating and stationary part offers significant advantages, such as low friction, high degree accuracy of motion, and zero wear. Balancing masses are used to properly balance the air-bearing platform. An inertial measurement unit (IMU), which comprises three gyroscopes, one per axis, is used to record angular rate measurements of the rotating platform. The experiments involve performing two maneuvers: a single-axis maneuver where two CMGs are used and a single-axis maneuver where four CMGs are used. The air-bearing design only allows free rotation about the vertical (z) axis and therefore the CMGs can only be used to demonstrate single-axis maneuvering. The experimental setup of the CMG cluster is depicted in Fig. 4.

The experiments were conducted in the University of Surrey's propulsion laboratory of the Surrey Space Centre. The CMGs used in the experiment are all identical and are placed in a pyramid geometrical configuration with a skew angle of 54.7 deg. The CMG electronics are positioned together with the CMG hardware and the only wires attached are the CAN bus, IMU serial link, and power cables. Figure 5 indicates a block diagram of the experiment performed.

Single Axis Maneuver with Two CMGs

The theoretical values for the CMG torques are measured using Eq. (2) in a CMG-based attitude control model simulated in MATLAB®/SIMULINK®.[1] The experimental values are measured via the relationship derived from the dynamics of the rotation table:

$$N_{\mathrm{CMG}} + N_d = -I_{\mathrm{AB}}\dot{\omega}_{\mathrm{AB}} \tag{4}$$

For $N_d = 0$ (due to the air-bearing table) and by knowing the moment of inertia of the air-bearing table, I_{AB} ($0.8\,\mathrm{kg}\cdot\mathrm{m}^2$), the experimental measurements of the angular rate ω_z can be used to calculate the experimental torque of the CMG cluster as seen in the block diagram

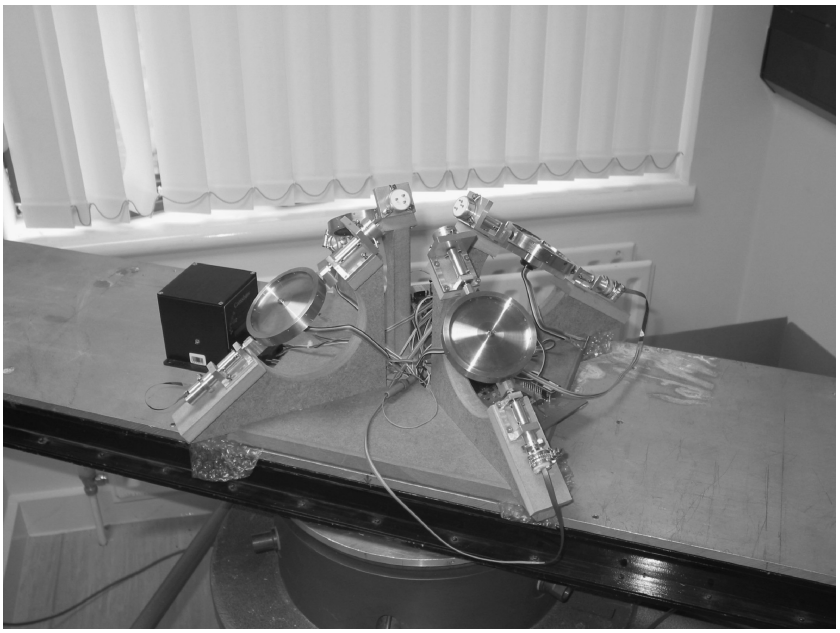

Fig. 4 CMG cluster experimental setup.

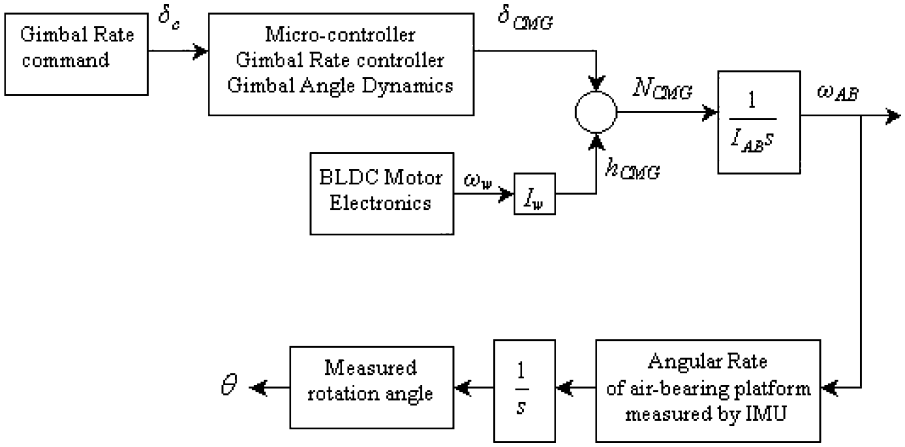

Fig. 5 Block diagram of the CMG cluster experiments.

Table 1 CMG Mk II characteristics

Parameter	Value
DC motor mass (Faulhaber 1525E)	30 g
Momentum wheel	150 g
Gimbal motor mass (P10)	9 g
Gimbal motor gear box (R10)	6 g
Potentiometer (sector)	10 g
Couplers (2)	10 g
CMG cluster power (Min.-Max.)	TBD[a]
Voltage	5–12 V
CMG mass	200 g
CMG h_0 ($\omega_w \sim 11{,}200$ rpm)	0.23 N · m · s
CMG avionics	50 g
CMG total mass	∼1170 g
CMG output torque	52.5 mN · m

[a]TBD, to be determined.

of Fig. 5. Table 1 presents the CMG design parameters and cluster characteristics.

Experimental Results and Discussion

Figure 6a indicates the theoretical and experimental CMG torques. Because of differentiation of the angular rates, the experimental value for torque starts from zero. The theoretical values are generated from CMG simulations modeled in MATLAB/SIMULINK, which do not take under consideration the wheel and gimbal motor dynamics or any other internal disturbances. The error between the two curves reaches a maximum of 0.006 N · m and this is mainly due to the disturbances that affect the CMG cluster on the air bearing (air-bearing bias, friction) and also due to mechanical reasons (CMG stepper motor backlash, microvibrations, misalignments, wheel imbalances, and small wheel-speed variations). The most dominating sources of error are those caused by aerodynamic friction and due to air-bearing biases. It is also the aerodynamic friction that does not allow the flywheel to output its complete output speed of 20,000 rpm; rather it outputs ∼11,200 rpm. For the mechanical errors, although they are high-bandwidth disturbances, they can potentially cause small errors in measurement. The IMU sampling is of the order of 1 s. Figure 6b presents the angular rates (measured and simulation values) with a maximum angular rate of 17.4 deg/s (experimental) and a maximum theoretical value of 18.6 deg/s. Multiple measurements were made and an average measurement set was used, from ten attempts, for all experiments presented in this work. The measurements were taken using small sampling rates due to the high angular rates of the rotating platform. The small errors between theoretical and experimental data can be explained from the disturbances mentioned. These errors are within a band of ±0.8 deg/s. Figure 6c illustrates the values for the angle θ, the rotation angle of the rotating air-bearing platform caused

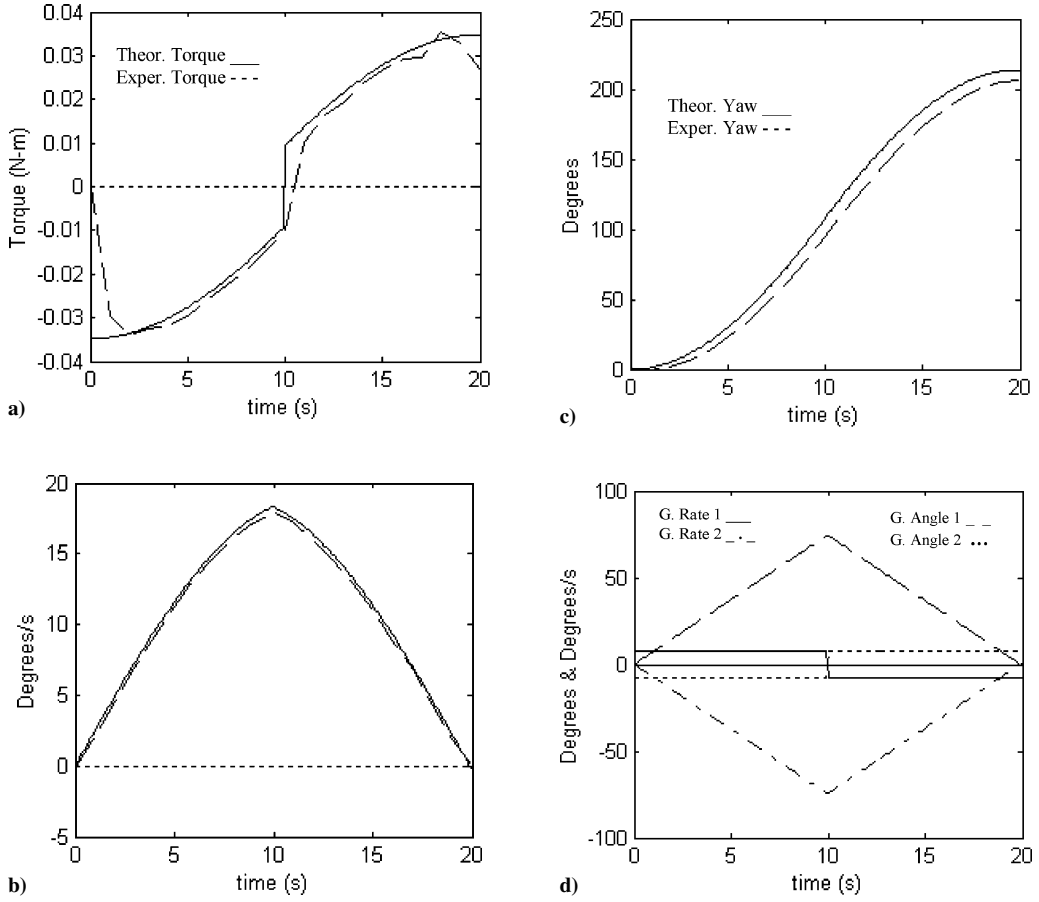

Fig. 6 a) Theoretical vs experimental CMG torque, b) theoretical vs experimental angular rate ω_z (yaw), c) theoretical vs experimental yaw (yaw), and d) gimbal angles and gimbal rates (theoretical).

by the CMG gimbaling. The angle θ expected from simulations is 218.4 deg, whereas the experimental value attained is 209.8 deg. Considering that the maneuver performed is an open-loop maneuver, and coupling the disturbance effects of the air-bearing, this result is within an acceptable error of 8.6 deg. This error in angle θ is expected to significantly decrease if the experiments were to be performed in a more ideal environment (clean room or in vacuum). However, even with the mentioned disturbances and expected small error in the rotation angle θ, the experiments demonstrate the CMG performance for a 0.8 kg $\cdot$ m^2 platform along with the significant torque capability of the CMGs. Figure 6d depicts the gimbal rates fed to the CMG system by the gimbal stepper motors with values of ± 7.5 deg/s, which generate gimbal angle excursions of ± 75 deg.

Single-Axis Maneuver with Four CMGs

The previous maneuver represents the minimum case for a single-axis maneuver about the x axis, where two CMGs are used. The next maneuver to be investigated is for a maneuver about the z axis, a case in which, due to the CMG cluster arrangement, all four CMGs are used to complete the maneuver. The total CMG torque about the z axis, $\boldsymbol{N}_z$, can be calculated as

$$\boldsymbol{h}_1 = h_0 \begin{bmatrix} -\cos\beta\sin\delta_1 \\ \cos\delta_1 \\ \sin\beta\sin\delta_1 \end{bmatrix}, \qquad \boldsymbol{h}_2 = h_0 \begin{bmatrix} -\cos\delta_2 \\ -\cos\beta\sin\delta_2 \\ \sin\beta\sin\delta_2 \end{bmatrix}$$

$$\boldsymbol{h}_3 = h_0 \begin{bmatrix} \cos\beta\sin\delta_3 \\ -\cos\delta_3 \\ \sin\beta\sin\delta_3 \end{bmatrix}, \qquad \boldsymbol{h}_4 = h_0 \begin{bmatrix} \cos\delta_4 \\ \cos\beta\sin\delta_4 \\ \sin\beta\sin\delta_4 \end{bmatrix}$$

$$\dot{\boldsymbol{\delta}}_1 = \begin{bmatrix} \dot{\delta}_1\sin\beta \\ 0 \\ \dot{\delta}_1\cos\beta \end{bmatrix}, \qquad \dot{\boldsymbol{\delta}}_2 = \begin{bmatrix} 0 \\ \dot{\delta}_2\sin\beta \\ \dot{\delta}_2\cos\beta \end{bmatrix}$$

$$\dot{\boldsymbol{\delta}}_3 = \begin{bmatrix} \dot{\delta}_3\sin\beta \\ 0 \\ -\dot{\delta}_3\cos\beta \end{bmatrix}, \qquad \dot{\boldsymbol{\delta}}_4 = \begin{bmatrix} 0 \\ \dot{\delta}_4\sin\beta \\ -\dot{\delta}_4\cos\beta \end{bmatrix}$$

The cross product of each of the CMG terms provides the torque generated per CMG ($\boldsymbol{N}_{\mathrm{CMG}-i}$). The sum of CMG torques about the z axis is, thus,

$$\boldsymbol{N}_z = \sum_{i=1}^{4} h_0\dot{\boldsymbol{\delta}}_i \sin\boldsymbol{\beta}\cos\boldsymbol{\delta}_i \tag{5}$$

Because of symmetric rotation, $\dot{\delta}_1 = \delta_2 = \delta_3 = \delta_4 = \boldsymbol{\delta}$ and $\dot{\delta}_1 = \dot{\delta}_2 = \dot{\delta}_3 = \dot{\delta}_4 = \dot{\delta}$

$$N_z = 4h_0\dot{\delta}\sin\beta\cos\boldsymbol{\delta} \tag{6}$$

Thus, for $\dot{\delta}_{\max} = 0.12$ rad/s and $\boldsymbol{\delta} = 0$ deg, $h_0 = 0.35$ N $\cdot$ m $\cdot$ s and $N_z = 0.13712$N $\cdot$ m; however, due to aerodynamic friction, the expected (measured) angular momentum available is $h_0 = 0.23$ N $\cdot$ m $\cdot$ s. Thus, the expected torque (expected from the CMG experiment) would be about $N_z = 0.09389$ mN $\cdot$ m. Consequently, the advantage in torque capability about the z axis of the CMG pyramid can be further utilized when CMGs are potentially used in a space mission by aligning the z axis of the pyramid cluster with the axis of most interest in the spacecraft (or body) coordinate frame (e.g., pitch axis). The increased torque capability can be used not only for increased performance but also for redundancy

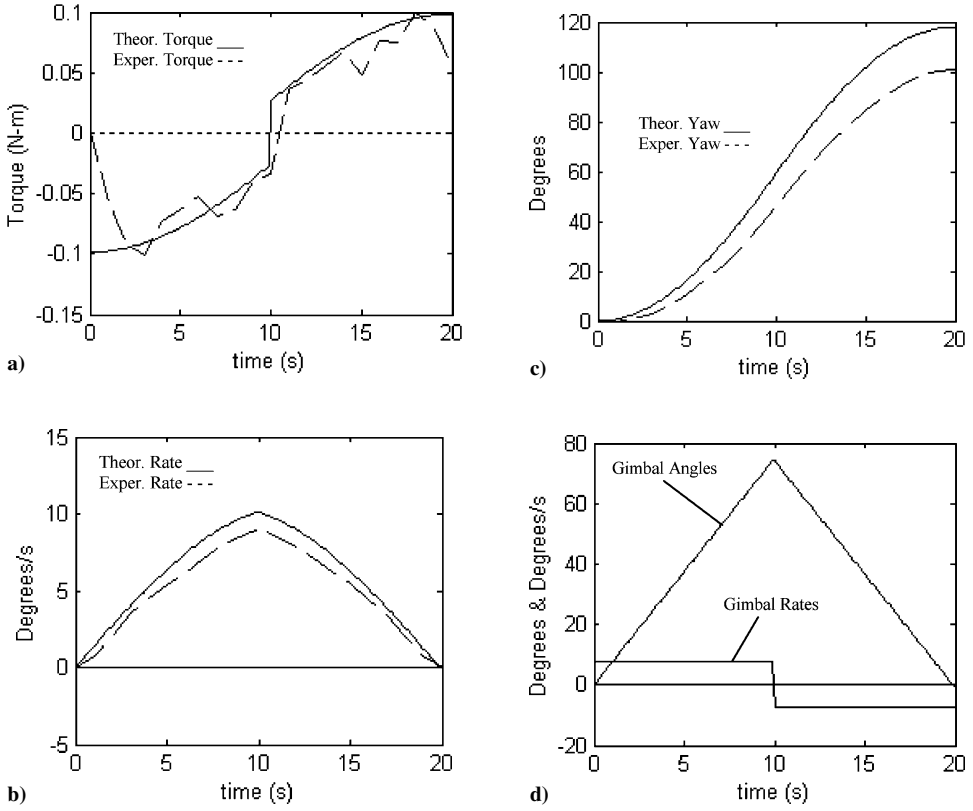

Fig. 7 a) Theoretical vs experimental CMG torque, b) theoretical vs experimental angular rate ω_z (yaw), c) theoretical vs experimental yaw (yaw), and d) gimbal angles and gimbal rates (theoretical).

(use of two CMGs). Figure 7 indicates a number of findings for the maneuver about the z axis. Similar to Fig. 6a, Fig. 7a presents the torque generated by the cluster of four CMGs used in this maneuver. A torque of 0.09389 N · m is expected and, although this torque is achieved during the practical experiments, expected errors are encountered during the maneuver reaching levels within the ±0.018 N · m band. These errors are mainly due to the same error sources as explained in the previous experiment. Because of the use of a cluster of four CMGs, these errors are expected to be amplified. Figure 7b shows the theoretical and experimental air-bearing platform angular rates, which achieve a maximum of 10.11 deg/s and 8.41 deg/s, respectively. In this second air-bearing experiment, a different platform inertia is used with an inertia I_{AB} of 4.1 kg · m^2. The larger rotating platform is preferred to the lighter platform used in the previous experiment in order to sustain better possible residuals of unbalance disturbances. Figure 7c indicates the rotation angle θ was measured by using the IMU, resulting in a value of 101.7 deg. The value expected through simulations is 118.8 deg. Similar to the previous experiment, Fig. 7d presents the cluster CMG gimbal rates and gimbal-angle excursions. The gimbal rates used are 7.5 deg/s and thus the gimbal-angle excursions reach a maximum of 75 deg in 10 s.

Sources of Experimental Errors

Analysis of the results from the experiments conducted show that there are three main sources of error causing variations between the theoretical and experimental results. These are aerodynamic friction, air-bearing biases, and high-frequency disturbances caused due to mechanical reasons.

The first source of error that was analyzed was aerodynamic friction. The experiments conducted were made in a clean environment but still with the presence of air. Testing of the flywheels in such an environment indicated a variation in the output speed of a value of ±150 rpm, which translates to a variation of 0.0026 N · m · s of angular momentum. The variation in angular momentum, which is 0.74% of the total angular momentum (0.35 N · m · s) but 1.15% of the operational angular momentum (0.23 N · m · s at 11,200 rpm), varies during experiments, which is a known quantified source of error.

Table 2 CMG vibration characteristics (maximum values) at the peak frequencies

Frequency, Hz	Harmonic	PSD, g^2/Hz	Acceleration, ms^{-2}	Force, m · N
15.22	1	4.6 (10^{-7})	1.1 (10^{-2})	11.2
142	8	9.2 (10^{-6})	4.9 (10^{-2})	60.1
202	12.5	1.9 (10^{-4})	0.31	261.7
601.6	39	9.0 (10^{-3})	2.11	1435.2

To further quantify the measurement noise, a CMG vibration (jitter) test was conducted using a triaxial accelerometer. The CMG flywheel was operated at 11,215 rpm and a power spectral density (PSD) response was attained, giving the results presented in Table 2. Ten readings were attempted with gimbal-angle discursions of ±180 deg and a gimbal rate of 7.5 deg/s. The results of Table 2 are averaged from ten sets of measurements. From the PSD measurements it is clear that the wheel shows vibration peaks at various frequencies. The first important frequency is at 15.22 Hz and is related to the wheel disk imbalance. The latter frequency peaks are associated with high-bandwidth disturbances that could belong to the following categories: gimbal dynamics, COTS bearings and lubrication, couplers, and mechanical misalignments. A more detailed analysis of these high-bandwidth disturbances would be necessary for flight hardware, especially for bearing- and lubrication-related issues. Bearing lifetime and performance issues are very important for the performance of actuators such as CMGs. The current CMG is an engineering model, which is used to demonstrate a near-space-rated CMG cluster for spacecraft with a high flywheel speed (>15,000 rpm) and low gimbal rate. Future CMGs, including the BILSAT CMG[3] currently in orbit, use knowledge gained from research such as the experiments presented in this paper and have

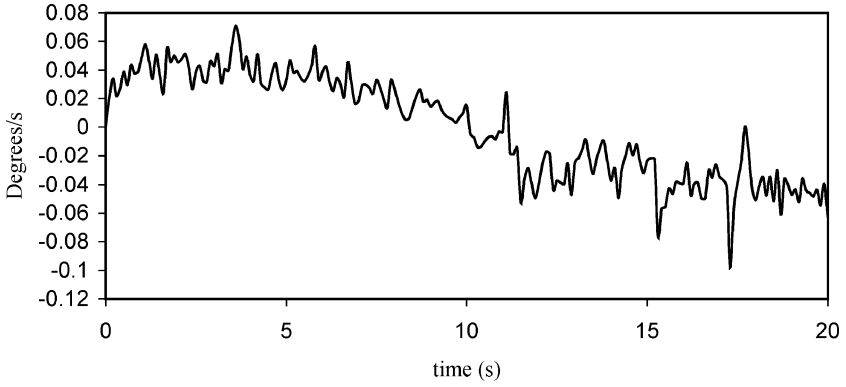

Fig. 8 IMU noise during 20-s maneuver.

improved designs with lower flywheel speeds, bearings with analyzable characteristics, and are enhanced though compact mechanical designs. Bearing issues for COTS dc brushless motors appear to have an important role in causing disturbances to the performance and resolution of a CMG and are currently analyzed for future CMG actuators currently in design.

Another important source of error is the noise that is caused by the gyro measurements made using the IMU. For the aforementioned two experiments, a sampling rate of 1 s was used. In the next experiment, a single-axis 40-deg maneuver using two CMGs is performed using a smaller IMU sampling rate of 0.1 s. To complete a single-axis 40-deg maneuver in 20 s (for the air-bearing platform inertia I_{AB} of 4.1 kg $\cdot$ m^2), a slightly higher gimbal rate of 7.75 deg/s is used and, thus, the gimbal-angle excursions reach a maximum of 77.5 deg in 10 s. The noise from the gyro measurements is quantified and presented in Fig. 8 for the experiment that follows.

Single-Axis Maneuver with Four CMGs with Filtering

Due to the noise caused from the gyro measurements, the angular rate measurements need to be filtered to reduce the noise and improve the accuracy of the measurements. In this case a Kalman filter is used.[9,10] As seen in Fig. 7d, the angular rate increase for 10 s, reach a maximum, and then decrease for 10 s where the maneuver is completed.

Thus, we use two similar Kalman filters for each phase. First we assume

$$\boldsymbol{\omega} = \boldsymbol{\omega}_0 + \dot{\boldsymbol{\omega}}\Delta t + \boldsymbol{q}_\omega \tag{7}$$

$$\dot{\boldsymbol{\omega}} = \dot{\boldsymbol{\omega}}_0 + \dot{\boldsymbol{q}}_\omega \tag{8}$$

The values that need to be filtered are the angular rate $\boldsymbol{\omega}$ and angular acceleration $\dot{\boldsymbol{\omega}}$. First we propagate the state vectors:

$$\bar{\omega}_k = \hat{\omega}_{k-1} + \hat{\dot{\omega}}_{k-1}\Delta t, \qquad \bar{\dot{\omega}}_k = \hat{\dot{\omega}}_{k-1} \tag{9}$$

where $k = 1, 2, 3, \ldots, n$ is the time of the first phase of the maneuver.

Then we propagate the covariance matrix,

$$\bar{\boldsymbol{P}}_k = \begin{bmatrix} 1 & \Delta t \\ 0 & 1 \end{bmatrix} \hat{\boldsymbol{P}}_{k-1} \begin{bmatrix} 1 & 0 \\ \Delta t & 1 \end{bmatrix} + \begin{bmatrix} q_\omega & 0 \\ 0 & \dot{q}_\omega \end{bmatrix} \tag{10}$$

which can also be written as

$$\bar{\boldsymbol{P}}_k = \begin{bmatrix} \bar{P}_{11} & \bar{P}_{12} \\ \bar{P}_{21} & \bar{P}_{22} \end{bmatrix}$$

Then we compute the Kalman gain[9,10]:

$$\boldsymbol{K} = \boldsymbol{P}\boldsymbol{H}^T(\boldsymbol{H}\boldsymbol{P}\boldsymbol{H}^T + \boldsymbol{R})^{-1} \tag{11}$$

Table 3 Kalman filter parameters

Parameter	Value
$\hat{\omega}_0$	0 rad/s
$\hat{\dot{\omega}}_0$	0 rad/s^2
P_{11}	3.046×10^{-6} (rad/s)^2
P_{22}	3.0276×10^{-9} (rad/s^2)^2
q_ω	3.046×10^{-6} (rad/s)^2
$\dot{q}_\omega$	3.0276×10^{-12} (rad/s^2)^2
R	6.092×10^{-6} (rad/s)^2

where $\boldsymbol{H}$ is the observation matrix; $\boldsymbol{H} = [1\ \ 0]$. Thus, the Kalman gain is

$$\boldsymbol{K}_k = \frac{1}{(\bar{\boldsymbol{P}}_{11} + R)} \begin{bmatrix} \bar{\boldsymbol{P}}_{11} \\ \bar{\boldsymbol{P}}_{21} \end{bmatrix} = \begin{bmatrix} \boldsymbol{K}_{11} \\ \boldsymbol{K}_{21} \end{bmatrix} \tag{12}$$

The state vectors are then updated:

$$\hat{\omega}_k = \bar{\omega}_k + \boldsymbol{K}_{11}(\omega_k - \bar{\omega}_k), \qquad \hat{\dot{\omega}}_{k-1} = \hat{\dot{\omega}}_{k-1} + K_{21}(\omega_k - \bar{\omega}_k) \tag{13}$$

Finally, the covariance matrix is updated as follows:

$$\hat{\boldsymbol{P}}_k = \begin{bmatrix} 1 - \boldsymbol{K}_{11} & 0 \\ -\boldsymbol{K}_{21} & 1 \end{bmatrix} \bar{\boldsymbol{P}}_k \tag{14}$$

As explained, a similar Kalman filter is used for the second phase of the maneuver ($10 \le t_k < 20$) but with the following modifications:

$$\bar{\omega}_k = \hat{\omega}_{k-1} - \hat{\dot{\omega}}_{k-1}\Delta t + \boldsymbol{q}_\omega, \qquad \bar{\dot{\omega}}_k = \hat{\dot{\omega}}_{k-1} + \dot{\boldsymbol{q}}_w \tag{15}$$

Then we propagate the covariance matrix as follows:

$$\bar{\boldsymbol{P}}_k = \begin{bmatrix} 1 & -\Delta t \\ 0 & 1 \end{bmatrix} \hat{\boldsymbol{P}}_{k-1} \begin{bmatrix} 1 & 0 \\ -\Delta t & 1 \end{bmatrix} + \begin{bmatrix} q_\omega & 0 \\ 0 & \dot{q}_\omega \end{bmatrix} \tag{16}$$

For the single-axis maneuver, the initial values used are presented in Table 3. Values for angular rate measurement noise R, angular rate, and acceleration noise q_ω are selected based on the observed noise levels and are refined heuristically.

Figure 9a illustrates the torque profile generated for the single-axis 40-deg maneuver. There are three profiles: the theoretical CMG torque is marked as a solid line, the raw measurement (or unfiltered) torque as a dashed line, and the filtered torque as a dash-dot line. The unfiltered torque clearly is very noisy, mainly due to the more pronounced effect of angular rate noise, especially after the differentiation of the angular rate that is needed to calculate the torque. Figure 9b presents more clearly the theoretical and the filtered experimental torques and Figure 9c illustrates the torque noise (caused by the gyro noise differentiated). The filtered, measured, and theoretical angular rates are shown in Fig. 9d. The CMGs rotate the air-bearing platform to an angle of approximately 37.89 deg (Fig. 9e). This, compared to the theoretical simulations, indicated an error in attitude (yaw) of 2.11 deg or 5.275%. Figure 9f presents the gimbal rate

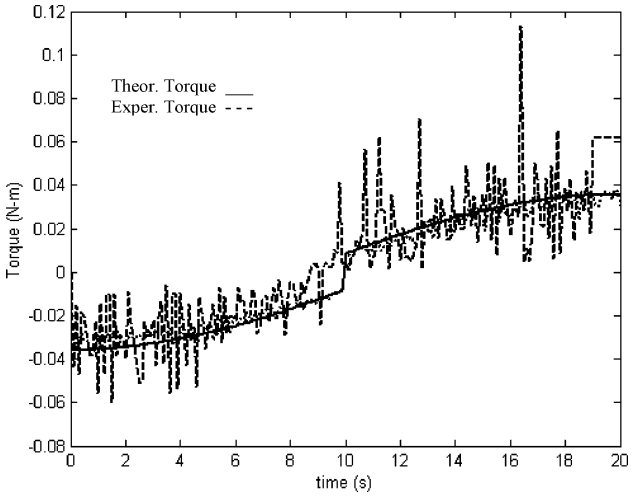

Fig. 9a Theoretical vs experimental CMG torque.

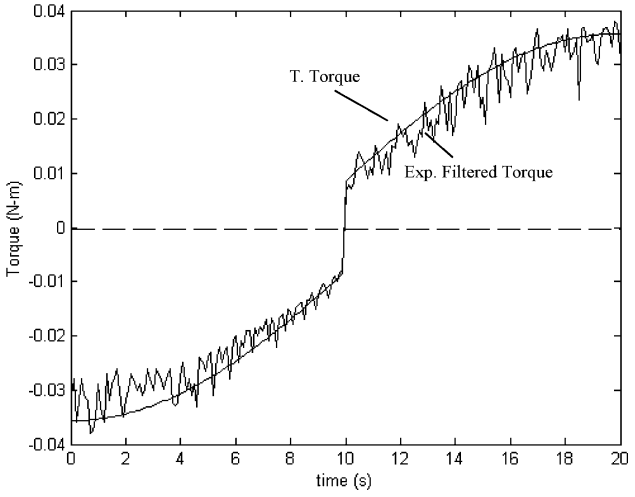

Fig. 9b Theoretical vs filtered experimental CMG torque.

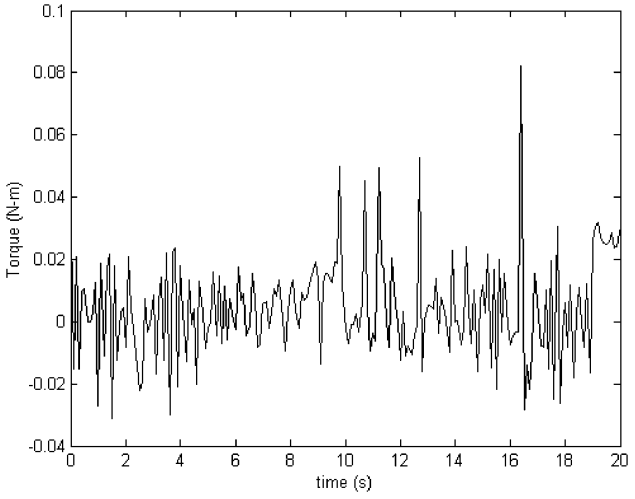

Fig. 9c CMG torque noise.

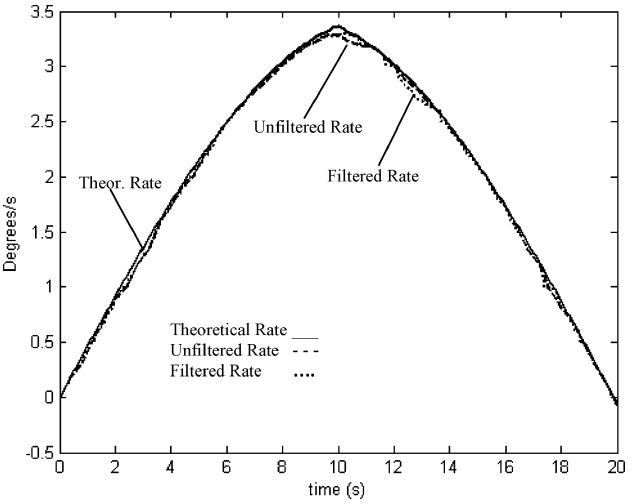

Fig. 9d Theoretical, unfiltered, and filtered angular rate ω_z (yaw).

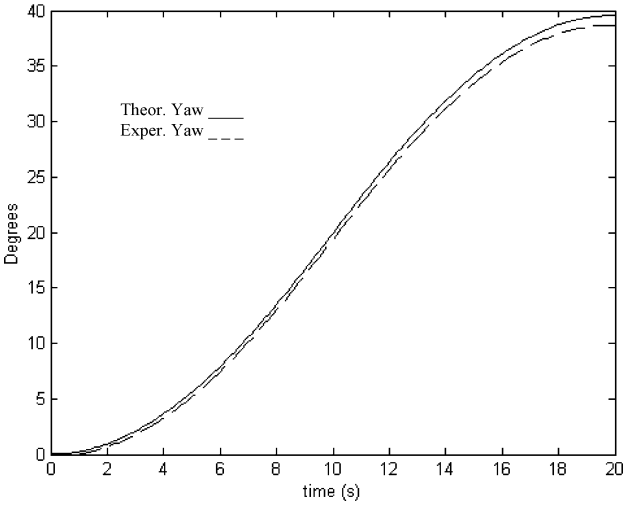

Fig. 9e Theoretical vs experimental angle (yaw).

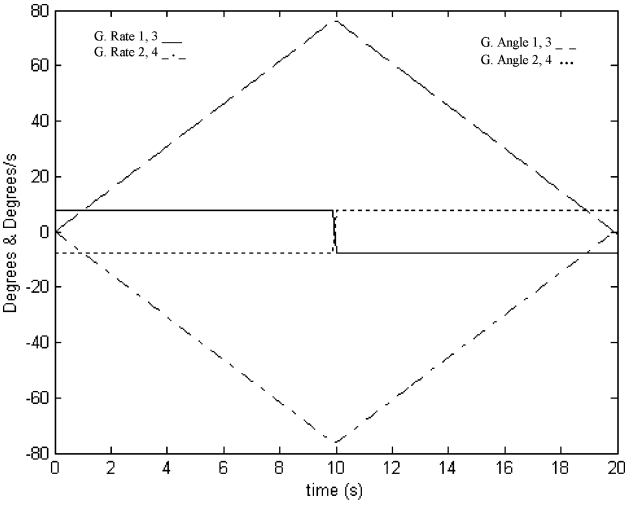

Fig. 9f Gimbal angles and gimbal rates (theoretical).

of ±7.75 deg/s as well as the maximum gimbal-angle excursions of ±77.5. The 40-deg maneuver used in this experiment is also used in the following paragraph to compare the power consumption of a CMG system to an RW system.

CMG Electrical Power Consumption

Electrical power is an issue critical in small satellite development and operations. Although some sources in the literature such as Schaub et al.[11] mention that CMGs require less electrical power than other actuators such as reaction/momentum wheels, there is no theoretical or practical support for this claim. The development of the CMGs in this paper as well as the information available on the reaction wheels developed at the University of Surrey can provide an indicative and practical means of comparing two different actuators, CMGs and RWs. The CMG Mk II was designed to be capable of producing a torque of 52.25 mN · m, which is sufficient

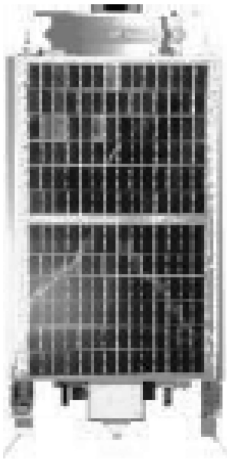

Fig. 10 University of Surrey's 50-kg-microsatellite platform.

to generate an average slew rate of 3 deg/s for the microsatellite platform (Fig. 10) analyzed in this paper.

Practical Comparison of Electrical Power Consumption

The following section provides a practical insight into trying to measure the electrical power consumption of the CMG cluster and then compares it with two different RWs. Although the comparison is not exact due to the lack of having equally torque-capable actuators in orbit (20 mN · m minisatellite RW and 5 mN · m microsatellite RW) as the CMGs, the comparison provides realistic and practical data on the power efficiency and advantage when utilizing a CMG system.

CMG Electrical Power Consumption

The actuator comparison is made based on using the CMG cluster conducting a single-axis yaw maneuver on the air-bearing table on which two CMGs are operated. This CMG operation is then compared to two single RW in-orbit performances, one using the minisatellite UoSAT-12 RW and another microsatellite RW from the Tsinghua-1 microsatellite. The basis of the electrical power comparison of the actuators (CMG vs RW) is the completion of the same single-axis maneuver of 40 deg, with one RW per case (minisatellite and microsatellite RWs) and two CMGs. For the CMGs, similar to the previous experiments, a 20-s bang-bang gimbal-angle maneuver is performed with a gimbal rate of 7.75 deg/s and, thus, the gimbal-angle excursions reach a maximum of 77.5 deg in 10 s and the maneuver is completed in 20 s. This slightly larger gimbal rate enables the completion of the required 40-deg maneuver in 20 s. The electrical power is measured by measuring the current used by the gimbal motors and flywheel motors, in vacuum. A vacuum jar is used to simulate the space environment as closely as possible, by using a pump to generate a pressure of 20 mbar (0.0194 atm).[1] Space is considered to have a pressure of approximately 10^{-7} torr, which is 1.35×10^{-4} bar (1.31×10^{-4} atm).[1] Although the pressure measured in the vacuum jar does not reach that in space (this would require using vacuum chambers, which are very expensive facilities), it is substantially better (only 1%) than operating the motors in a 1-atm environment. For electrical power consumption of motors, because the CMG cluster is operated in a 1-atm environment, it is important to measure the motor current in vacuum to avoid measuring the extra power that would be required to fight aerodynamic friction that would exist in the 1-atm environment. This would make the electrical power consumption comparison of the CMGs, versus RWs in orbit, more realistic. Figure 11 shows the two-CMG cluster's maximum and average powers to be 1.614 and 1.617 W, respectively, when performing a single-axis maneuver.

Reaction Wheel Electrical Power Consumption

Next, two cases of RW-based maneuvers of different size (microsatellite and minisatellite) are presented. Table 4 details the specifications of the two RWs. First, an experiment to show the electrical power consumption of the Tsinghua-1 microsatellite RW is

Table 4 Minisatellite and microsatellite RW characteristics

Reaction wheels	Manufacturer	Angular momentum, N · m · s	Power range, W	Torque range, N · m
Tsinghua-1 RW	3 SSTL[a] units (X/Y/Z)	±0.36 @ ±5000 rpm	0.2-3 (zero to max. accel.)	±0.01 max
UoSAT-12 RW	3, (2) SSTL, (1) Ithaco units (X/Y/Z)	±4 @ ±5000 rpm	2.8-14.6 (zero to max. accel.)	±0.02 max

[a]SSTL, Surrey Satellite Technology, Ltd.

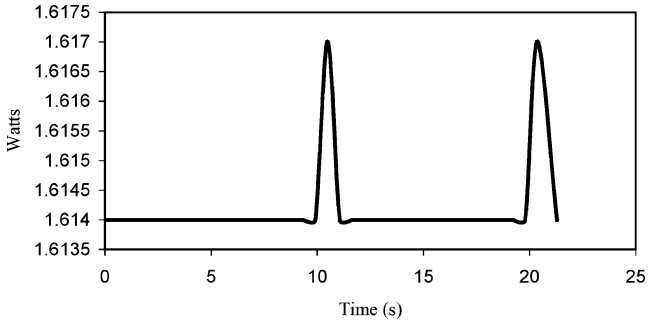

Fig. 11 Two-CMG cluster electrical power consumption.

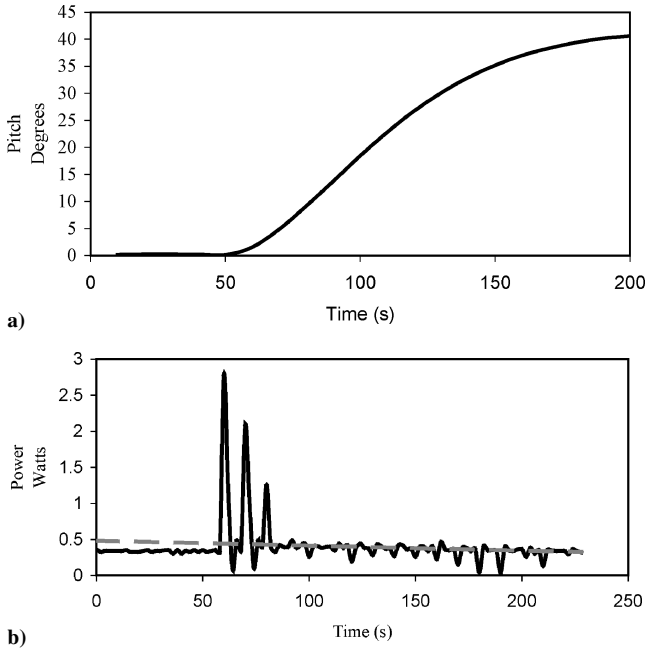

Fig. 12 Absolute electrical power consumption: Tsinghua-1 a) pitch maneuver and b) RW.

conducted. A 40-deg pitch maneuver is commanded to be completed. For Tinghua-1, a microsatellite with a mass of 50 kg, the maneuver is completed in 150 s. Figure 12a illustrates the maneuver requested from data received via Tsinghua-1 telemetry on 9 September 2002. The torque is calculated using the following equation:

$$N_{\mathrm{RW}} = I_{\mathrm{RW}} \dot{\omega}_W \tag{17}$$

where I_{RW} is the inertia of the flywheel with a value of 4×10^{-4} kg · m^2. Figure 12b indicates the absolute electrical power consumption of the RW during the maneuver. The maximum electrical power occurs during the maximum acceleration of the flywheel, and its peak power reaches a value of 2.87 W. The average of the absolute electrical power during the maneuver is 0.45 W. The power measurement is still not the overall maximum value of the RW because

Table 5 Electrical power consumption data comparison

Satellite	Inertia, $kg \cdot m^2$	Time, s	Torque, $mN \cdot m$	Mass, kg	Av. power, W	Scaled power, $W \cdot kg \cdot m^2$	Scaled energy, $J/kg \cdot m^2$
UoSAT-12	40	200	20	3.2	2	0.05	10
Tsinghua-1	2.5	150	10	1	0.45	0.18	27
CMG	4.1	20	52.25	0.59*	1.61	0.39	7.85

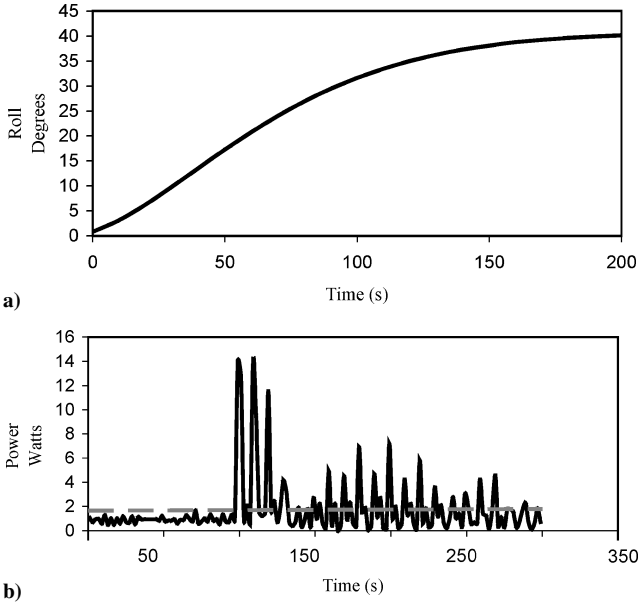

Fig. 13 Absolute electrical power consumption: UoSAT-12 a) roll maneuver and b) RW.

the wheel is not accelerating at its maximum acceleration capability on this 40-deg maneuver. Similar to Tsinghua-1, the UoSAT-12 minisatellite is used to compare electrical power consumption for the two-CMG cluster. In this experiment, a single-axis 40-deg roll maneuver is commanded using one of the Surrey RWs. Figure 13a depicts the 40-deg maneuver. For UoSAT-12, I_{RW} is the inertia of the flywheel, with a value of 7.7×10^{-3} kg · m^2. Torques of 19.1 mN · m are required for short acceleration times. Figure 13b indicates the absolute electrical power consumption of the RW. One can notice the instantaneous peaks in electrical power required to accelerate the flywheel. The average electrical power for this maneuver is near 2 W, whereas the maximum power exceeds 14 W.

Electrical Power Consumption Discussion

A series of experiments was conducted to determine and compare the electrical power consumption of CMG and RW systems. Although this comparison is not exact due to the unavailability of an RW that can produce a 52.25 mN · m torque, which the CMGs can produce, the results attained from the experiments provide useful information toward proving that CMGs are more efficient from an electrical power consumption point of view than RW systems. Table 5 summarizes the data attained from the electrical power experiments of the RW and CMG actuators, all performing a single-axis 40-deg maneuver. The mass of two CMGs is 0.59 kg and does not take into account shielding as with the RWs. Clearly the CMGs rotate the air-bearing platform (4.1 kg · m^2) rapidly, in 20 s. As mentioned before, the task of comparing different actuators on different platforms is challenging. A scaled power index is introduced to measure the power per kg · m^2 that each actuator consumes. To compare the actuators in an equal way, an energy index is introduced. The index reflects the energy accumulated during a maneuver on a normalized 1 kg · m^2 moment of inertia (MOI) platform. This makes the comparison for all actuators for the same-single axis 40-deg maneuver compatible because the platforms are of different size. The index takes into account the slew rate (and thus torque) capability of the actuators: the power required to perform the same single-axis 40-deg maneuver for all actuators "using" the same platform (normalized 1 kg-m^2). The index referred to as a scaled energy index is simply the work (power multiplied by the time needed to complete the maneuver) divided by each spacecraft's MOI:

$$\varepsilon = P_{\text{act}} t_m / I_s \tag{18}$$

From Table 5, the CMGs prove to be the least power-consuming actuator with an energy index of 7.85. This is 21.5% more efficient than the UoSAT-12 RW power consumption and 70.9% more efficient than the Tsinghua-1 RW. Thus, we can conclude that the CMGs have a power advantage over RWs and can be considered more power efficient actuators than RWs.

Conclusions

Practical work confirms the theoretical findings on the advantageous use and performance of CMGs for agile small satellites. A cluster of four CMGs in pyramid arrangement is used to demonstrate full three-axis control. Using an air-bearing platform, ground experiments were performed to evaluate the performance of the designed CMGs as well as to practically confirm the theoretical findings of previous CMG work. The CMG cluster is able to generate the required torque of 52.25 mN · m in order to provide an average slew rate of 3 deg/s for the microsatellite platform, which is analyzed in this paper. Two different single-axis maneuvers were made to replicate an x-axis maneuver using two CMGs and a z-axis maneuver using four CMGs for a spacecraft equipped with CMGs. Because of disturbances such as aerodynamic friction it was expected that the CMGs would not be able to achieve their full torque capability on ground tests in a 1-atm environment. However, the experiments indicated their large torque capability ranging from 36 mN · m for the two-CMG maneuver to 93.51 mN · m for the four-CMG maneuver. Furthermore, experiments indicate the superior electrical power efficiency when utilizing a CMG cluster compared to that for an RW system. Specifically, a two-CMG cluster's maximum and average powers were found to be 1.614 and 1.617 W, respectively, when performing a single-axis maneuver. In a comparison with two different RWs onboard two different small satellites currently in orbit, the CMGs are shown to be more power efficient by at least 21.5% from reaction wheels, with a mass saving of 41.5% to the smallest (Tsinghua-1) RW, while performing the same attitude maneuver. Having a total mass of about 1.17 kg (including all electronics), CMGs were shown in a practical way to potentially be an efficient and highly capable means of controlling agile small satellites.

References

[1]Lappas, V. J., "A Control Moment Gyro (CMG) Based Attitude Control System (ACS) for Agile Small Satellites," Ph.D. Dissertation, Surrey Space Center, University of Surrey, Guildford, England, U.K., Oct. 2002.

[2]Wie, B., *Space Vehicle Dynamics and Control*, AIAA Educational Series, AIAA, Reston, VA, 1998, pp. 437–444.

[3]Gomes, L., Yuksel, G., Lappas, V., da Silva Curiel, A., Bradford, A., Ozkaptan, C., and Sweeting, M., "BILSAT-1: Advancing Smallsat Capabilities," *17th AIAA/USU Small Satellite Conference Proceedings*, SSC03-VI-4, AIAA, Utah, Aug. 2000.

[4]Roser, X., and Sghedoni, M., "Control Moment Gyroscopes (CMG's) and Their Application in Future Scientific Missions," *Proceedings of the 3rd International Conference on Spacecraft Guidance, Navigation and Control Systems*, ESA, Noordwijk, The Netherlands, 1997, pp. 523–528.

[5]Defendini, A., Lagadec, K., Guay, P., Blais, T., and Griseri, G., "Low Cost CMG-Based AOCS Designs," *Proceedings of the 4th International Conference on Spacecraft Guidance, Navigation and Control Systems*, ESA, Noordwijk, The Netherlands, 2000, pp. 393–398.

[6]Blondin, J. C., " Small-CMG's: Needs, Capabilities, Trades and Implementation," *AAS/AIAA GNC Rocky-Mountain Conference*, American Astronautical Society, 1996.

[7]Defendini, A., Fauchex, P., Guay, P., Bangert, K., Heimel, H., Privat, M., and Seiler, R., "CONTROL MOMENT GYRO CMG 15-45 S: A Compact CMG Product for Agile Satellites in the One Ton Class," *Proceedings of the 10th European Space Mechanisms and Tribology Symposium*, ESA, San Sebastian, Spain, Sept. 2003.

[8]Abbott, B., "Honeywell's Small Control Moment Gyro Development," *26th Annual AAS Guidance and Control Conference*, American Astronautical Society, Breckenridge, CO, Feb. 2003.

[9]Kalman, R., "A New Approach to Linear Filtering and Prediction Problems," *Journal of Basic Engineering*, Vol. 82, Ser. D, March 1960, pp. 35–45.

[10]Brown, R. G., and Hwang, P. Y. C., *Introduction to Random Signals and Applied Kalman Filtering*, Wiley, New York, 1997, pp. 101–112.

[11]Schaub, H., Junkins, J. L., and Vadali, S. R., "Feedback Control Law for Variable Speed Control Moment Gyros," *Journal of Astronautical Sciences*, Vol. 46, No. 3, 1998, pp. 307–328.

C. Kluever
Associate Editor